RESEARCH PAPER

Multiparametric MRI in differentiating solitary brain metastasis from high-grade glioma: diagnostic value of the combined use of diffusion-weighted imaging, dynamic susceptibility contrast imaging, and magnetic resonance spectroscopy parameters

Kerim Aslan[1], Hediye Pinar Gunbey[2], Leman Tomak[3], Lutfi Incesu[1]

[1]Department of Radiology, Ondokuz Mayis University Faculty of Medicine, Samsun, Turkey

[2]Department of Radiology, Health Sciences University Kartal Lütfi Kırdar Training and Research Hospital, Istanbul, Turkey

[3]Department of Biostatistics, Ondokuz Mayis University Faculty of Medicine, Samsun, Turkey

This study was presented at the 26th Scientific Congress of the Turkish Neuroradiology Society,

17-19 February, 2017 in Istanbul, Turkey.

Abstract

Objective. The purpose of this study was to determine whether the combined use of diffusion weighted imaging (DWI), magnetic resonance spectroscopy (MRS), and dynamic susceptibility contrast imaging (DSCI) parameters could provide a more accurate diagnosis in the differentiation of high-grade glioma (HGG) from solitary brain metastasis (SBM) in the enhancing tumour and in the peritumoural region.

Materials and methods. Fifty-six patients who received DWI, DSCI, and MRS before surgery were assessed. In differentiating SBM from HGG, the cutoff values of the DWI-apparent diffusion coefficient (ADCmin, ADCmax, and ADCmean), DSCI-relative cerebral blood volume (rCBV), and MRS-Cho/Cr, Cho/NAA, and NAA/Cr parameters for the peritumoural region were determined with ROC. The combined ROC curve was used for the different combinations of the peritumoural region DWI, DSCI, and MRS parameters in differentiating between the two tumours, and the best model combination was formed.

All procedures performed in studies involving human participants were in accordance with the ethical standards of the institutional research committee and with the 1964 Helsinki Declaration and its later amendments. This study was approved by the Institutional Review Board at our institutes.

Results. In the enhancing tumour, all the parameters except NAA/Cr (P = 0.024) exhibited no statistical difference in differentiating between these two groups (P > 0.05). AUC values for ADCmin, ADCmax, ADCmean, rADCmin, rADCmax, rADCmean, rCBV, Cho/Cr, Cho/NAA, and NAA/Cr parameters in the peritumoural region in differentiating SBM from HGG were 0.860, 0.822, 0.848, 0.822, 0.801, 0.822, 0.906, 0.851, 0.903, and 0.784, respectively. In differentiating HGG from SBM, the best model consisted of the combination of peritumoural ADCmin, rCBV, and Cho/NAA parameters. AUC values were 0.970.

Conclusions. The combination of peritumoural region ADCmin, rCBV, and Cho/NAA parameters can help in differentiating SBM from HGG, with a diagnostic accuracy of 97%.

Key words: Solitary brain metastasis, high-grade glioma, diffusion-weighted imaging, dynamic susceptibility contrast imaging, magnetic resonance spectroscopy

(*Neurol Neurochir Pol 2019; 53 (3): 227–237*)

Address for correspondence: Kerim Aslan, Ondokuz Mayis University Faculty of Medicine, Department of Radiology, Kurupelit/Samsun, Turkey;
e-mail: mdkerim@hotmail.com, tel.: +90362 3121919- 2541, fax: +903624576041

Introduction

High-grade glial (HGG) tumours and brain metastases are the most frequently diagnosed brain tumours in adults. In the diagnosis of brain metastasis, primary malignancy history, multiple lesions, and the combined localisation of grey–white substance are helpful. However, in patients with primary malignancy, HGG can occur and can sometimes be multiple. In almost 30% of extracranial malignancies, the first manifestation of the disease can be solitary brain metastasis (SBM) [1, 2]. As SBM and HGG usually have similar signal intensities and contrasting patterns in conventional magnetic resonance imaging (MRI), MRI can be inadequate in differentiating between these two tumours [3, 4]. Treatment planning, follow up, and prognosis are different between SBM and HGG. In patients with malignancy, an enhancing brain lesion may not only be treated by surgical resection but also by radiotherapy since such a lesion may often be judged to be a metastasis without a histopathological assessment. In such cases, image-based differentiation could play an important role in the treatment choice. Therefore, reliable imaging is important in differentiating between these two tumours.

Whereas HGG has infiltrative neoplastic cells in the peritumoural oedema, the peritumoural region of SBM is characterised by vasogenic oedema depending on the increase in capillary permeability. Therefore, determining these changes in the peritumoural region is crucial in differentiating HGG from SBM. Apart from conventional MRI, advanced MR imaging modalities such as diffusion-weighted MRI (DWI), MR spectroscopy (MRS), and dynamic susceptibility perfusion MRI (DSCI) are used to identify these changes in the peritumoural region by providing quantitative measurements. Apparent diffusion coefficient (ADC) obtained from DWI provides information on the cellularity of the tissue by measuring independently from the direction of the total magnitude of water diffusion in the tissue. Some studies have shown that low ADC values are associated with high cellularity in the peritumoural region in HGG compared to SBM [5–14] Suh et al. [15] reported that DWI and diffusion tensor imaging (DTI) demonstrated a moderate diagnostic performance for the differentiation of high-grade glioma from solitary brain metastasis. Choline (Cho) metabolite in MRS reflects cellular density and the rate of cellular membrane turnover. Studies on MRS have shown increases in Cho/creatine (Cr) and Cho/N-acetyl aspartate (NAA) in the peritumoural region infiltration in HGG tumours, and reported that these increases could be used in differentiating them from metastases [16–20]. The relative cerebral blood volume (rCBV) obtained from DSCI provides a quantitative assessment of neovascularisation based on the tumour infiltration in the peritumoural region. Some studies have indicated that the high rCBV values associated with neovascularisation in the peritumoural region in HGG could be useful in differentiating between these two

tumours [21–25]. Suh et al. [26] reported that perfusion MRI shows high diagnostic performance in differentiating glioma from brain metastasis.

Some studies have used advanced MR modalities in differentiating SBM from HGG [27–31]. However, none of these works examined the difference between SBM and HGG by using a combination of these modalities. Recently, researchers have examined the uses of different combinations of advanced MRI techniques in differentiating between these two tumours. Some of these studies have shown that the combinations of diffusion and perfusion parameter measurements could be helpful in differentiating between these two tumours [32–35]. Tsolaki et al. [36] combined MRS and perfusion techniques with machine learning methods in differentiating between glioblastomas and solitary metastases, and reported that they provided additional diagnostic information in definitive diagnosis. Mouthuy et al. [37] showed that multimodal MRI parameters (perfusion–rCBV, texture parameter contrast, and sum average) could be useful in differentiating between SBM and HGG. Tsougos et al. [38] reported that the MRS and DSCI measurements of the peritumoural region could help differentiate between glioblastomas and metastases, whereas diffusion parameters could not statistically differentiate between the two lesions.

The purpose of this study was to determine whether the combined use of the DWI [minimum (ADCmin), mean (ADCmean), and maximum (ADCmax) ADC and minimum (rADCmin), mean (rADCmean), and maximum (rADCmax) ADC ratio], MRS (Cho/Cr, Cho/NAA, and NAA/Cr) and DSCI (rCBV) parameters could provide a more accurate diagnosis in differentiating SBM from HGG in the enhancing tumour and in the peritumoural region. Our purpose was also to reveal the diagnostic accuracy of both parameters in differentiating between these two tumours.

Materials and methods

Patients

This study was approved by the local ethics committee of our institution (OMÜ KAEK 2017/153). Preoperative MRI and clinical records of 86 consecutive patients who were referred to our hospital between March 2012 and December 2016 and who were diagnosed with brain metastasis and HGG histopathological were examined retrospectively. Several patients were excluded: two patients who had pre-resection stereotactic biopsy, two patients who had been treated, 11 patients who did not have a solitary lesion (HGG, n = 2 and BM, n = 9), four patients who did not have a peritumoural oedema in the lesion, and five patients who did not receive DWI, DSCI, and MRS. Patients with a lesion size smaller than 2 cm were also excluded from the study (n = 6). So eventually, 56 patients who did not receive pre-resection stereotactic biopsy and treatment, who had a solitary enhancing brain tumour and peritumoural oedema, and who received conventional

brain MRI, DWI, MRS, and DSCI were included in the study. The final diagnosis included 39 HGG (19 men, 20 women; mean age: 61.2 ± 10.5 years; range: 37–81 years) and 17 SBM (nine men, eight women; mean age: 61.0 ± 13.8 years; range: 29–83 years).

In 39 patients, the tumours were classified as HGG, including 11 with World Health Organisation (WHO) grade III (eight anaplastic astrocytoma and three anaplastic oligodendrogliomas) and 28 with WHO grade IV (glioblastomas) according to the WHO criteria. Metastatic brain tumours included lung carcinoma (n = 9), breast carcinoma (n = 3), melanoma (n = 1), renal carcinoma (n = 1), colon carcinoma (n = 1), ovarian carcinoma (n =1), and carcinoma of unknown origin (n = 1).

MR image acquisition

MRI imaging was performed using a 1.5-T scanner (Gyroscan Intera, Philips Healthcare, Best, the Netherlands) with an eight-channel head coil. Conventional MR imaging sequences, DWI, DSCI, and multivoxel MRS imaging were performed on all patients. Conventional MRI protocols included pre-contrast axial T1-weighted sequence (repetition time [TR]/echo time [TE]: 450/15 ms; slice thickness: 5 mm; field of view [FOV]: 230 mm; matrix: 256 × 163; number of excitations [NEX]: 2; intersection gap: 1 mm), axial T2-weighted sequence (TR/TE: 4,443/100 ms; section thickness: 5 mm; FOV: 230 mm; matrix: 384 × 240; NEX: 3; intersection gap: 1 mm), coronal fluid attenuation inversion recovery (TR/TE/TI: 8,000/140/2,800 ms; section thickness: 5 mm; FOV: 230 mm; matrix: 224 × 148; NEX: 2; intersection gap: 0.4 mm), sagittal T2-weighted sequence (TR/TE: 4,027/100 ms; section thickness: 5 mm; FOV: 230 mm; matrix: 236 × 205; NEX: 2; intersection gap: 1 mm).

DWI was performed with a single-shot spin-echo EPI (TR/TE: 3,376/74 ms; section thickness: 5 mm; FOV: 230 mm; matrix: 128 × 128; NEX: 2; intersection gap: 1 mm; b values: 0 and 1,000 s/mm^2).

DSCI was conducted using a single-shot spin-echo EPI sequence (TR/TE: 1,524/40 ms; section thickness: 5 mm; FOV: 230 mm; matrix: 128 × 128; NEX: 2; no gap; voxel size: 2.0 mm x 2.0 mm x 5.0 mm). All of the patients were given intravenous gadobutrol (0.05 mmol/kg, 1.0 mmol/mL, Gadovist; Bayer Schering Pharma, Berlin, Germany) in a preloading dose to decrease pre-dynamic imaging contrast agent leakage. DSCI was performed during the first pass of the standard dose (0.1 mmol/kg) bolus of an intravenous contrast agent (gadobutrol). The injection rate was 5 mL/s for all patients and was followed by a 20mL flush of saline at the same rate given through a power injector. Following the contrast injection, a post-contrast 3D T1-weighted sequence was performed (TR/TE: 500/4 ms; NEX: 1; slice thickness: 1 mm; no gap; in-plane resolution: 1 mm; FOV: 240 mm; voxel size: 1.0 mm x 1.0 mm x 1.0 mm).

MRS was conducted after contrast injection in all patients. For MRS imaging, a 3D multivoxel PRESS sequence was performed (automatic shimming and Gaussian water suppression; TR/TE: 988/144 ms; section thickness: 5 mm; FOV: 180 x 160 mm; matrix: 180 x 160; NEX: 2). The volume of interest (VOI) was chosen from the tumour, peritumoural region, and contralateral normal-appearing white matter, avoiding the scalp, skull base, and the sinuses. Saturation slabs were placed outside the VOI to suppress lipid signals from the scalp. VOI position was determined by examining the MR images in three plans (sagittal, coronal, and transverse). The size of the VOI differed according to the sizes of the lesions, and the most frequent was 80 x 80 mm. The voxel size was 10 × 10 × 10–15 mm.

Image analysis

All conventional MRI, DWI, DSCI, and MRS datasets were transferred to an independent workstation (IntelliSpace, software version v6.0.4.03700, Philips). Two neuroradiologists (K.A. and H.P.G., both with six years of experience) were unaware of the clinical and pathological results of the patients, and were completely independent of each other in the measurement of the DWI (ADCmin, ADCmax, ADCmean, rADCmin, rADCmax, and rADCmean), DSCI (rCBV), and MRS (Cho/Cr, Cho/NAA, and NAA/Cr) parameters with the regions of interest (ROIs).

ADC maps were acquired from DWI. ROIs were drawn manually in round or oval shapes in solid portions by avoiding the cystic, necrotic and calcified areas of lesions from ADC maps. These areas were identified in T2-weighted and contrast-enhanced T1W images. The peritumoural region was defined as the 1 cm T2 and FLAIR hyperintense area outside the contrasted area. Circular ROIs, which were drawn at workstations manually to lesions from T2-weighted images, were placed automatically to lesions on ADC maps with the same localisation and size. The peritumoural and tumoural ADC ratios were calculated by dividing the average ADCmin, ADCmax, ADCmean values of the peritumoural area and contrasted solid tumour by the average normal white matter ADCmin, ADCmax, and ADCmean values.

The arterial input function was selected automatically, and the CBV maps were calculated using the block-circulant singular value decomposition technique for DSCI [39]. CBV maps were formed for analysis at the workstation from DSCI perfusion datasets. The CBV maps were then coregistered to contrast-enhanced 3D T1-weighted images for the enhancing tumour and T2-weighted images for the peritumoural region. For the CBV measurements, ROIs were manually drawn by avoiding cerebral blood vessels, calcifications, haemorrhage, and cerebrospinal fluid-filled sulci areas. ROIs were placed carefully on each selected section of the CBV maps, including the areas of the enhancing tumour and the peritumoural region, with the highest CBV determined by visual inspection. The CBV values for the enhancing tumour and the peritumoural region were calculated. The peritumoural and enhancing tumour rCBV was determined by dividing the

average CBV values of the peritumoural area and enhancing tumour by the average CBV values of the lesion level of the contralateral normal area.

The 3D multivoxel PRESS spectroscopic data analysis and the calculation of the metabolite ratios were conducted at the workstation. The post-processing steps, including the frequency shift, baseline correction phase correction, and peak fitting/analysis, were performed automatically. The spectra were automatically analysed for the relative signal intensities (areas under the fitted peaks in the time domain) of metabolites. The maximum values of Cho/Cr and Cho/NAA ratios and the minimum NAA/Cr ratios were obtained from the spectral maps of three localisations (enhancing tumour, peritumoural region, and normal appearing white matter). Cystic or necrotic, calcific, and haemorrhagic areas of the tumour were avoided when choosing the voxel. To minimise the partial volume effect, the voxel was chosen without including the neighbouring peritumoural region as much as possible for the enhancing tumour and for the peritumoural region without including the T2 and FLAIR hyperintensity outside the peritumoural area and the enhancing tumour.

Statistical analysis

Statistical analyses were performed using the Statistical Package for the Social Sciences (IBM SPSS Statistics version 21; IBM, Armonk, NY, USA). Data were presented as the mean (SD), median (min–max), or frequency (%). To identify the differences between SBM and HGG in the enhancing tumour and the peritumoural region, we used Student's t-test for normally distributed data (age, ADCmin, ADCmax, ADCmean, rADCmin, rADCmax, rADCmean, rCBV, Cho/Cr, Cho/NAA, and NAA/Cr). The frequencies were compared using the continuity correction χ2. AUC was evaluated as the measure of a diagnostic test's discriminatory power. For the differentiation between SBM and HGG in the peritumoural region, the optimum cutoff values of the DWI (ADCmin, ADCmax, ADCmean, rADCmin, rADCmax, and rADCmean), DSCI (rCBV), and MRS (Cho/Cr, Cho/NAA, and NAA/Cr) parameters were determined using the ROC curve. The combined ROC curves were used for the combination of the peritumoural region DWI, DSCI, and MRS parameters in differentiating between the two tumours. The sensitivity, specificity, positive predictive value (PPV), and negative predictive value (NPV) were also identified. The AUC was calculated for the ROC curve of each individual classifier and for the combined ROC curves. The best model combination was then formed. The inter-observer agreement between two readers was assessed using weighted Cohen κ statistics. A κ value of 0.4 or lower indicates poor agreement; 0.41–0.60, moderate agreement; 0.61–0.80, good agreement; and 0.81–1.0, excellent agreement. A P value < 0.05 was considered significant.

Results

Figures 1 and 2 present the samples of our multiparametric MRI in patients with HGG and SBM, respectively.

The ADCmin, ADCmax, ADCmean, rADCmin, rADCmax, and rADCmean values and the NAA/Cr rates of HGG in the peritumoural region were significantly lower than those of SBM (P < 0.001, P < 0.001, P < 0.001, P < 0.001, P < 0.001, P < 0.001, and P = 0.009, respectively), and the rCBV, Cho/Cr, and Cho/NAA rates were significantly higher (P < 0.001). However, in the enhancing tumour, all the parameters except NAA/Cr (P = 0.024) exhibited no statistical differences in differentiating between these two groups (P > 0.05). The quantitative values, which include the mean ± SD and median (min-max) of all the parameters (ADCmin, ADCmax, ADCmean, rADCmin, rADCmax, rADCmean, rCBV, Cho/Cr, Cho/NAA, and NAA/Cr) in the enhancing tumour and the peritumoural region, the statistical analyses, and the κ coefficient values are summarised in Table 1 (enhancing tumour) and Table 2 (peritumoural region).

Table 3 presents the cutoff, sensitivity, specificity, PPV, NPV, and AUC values for each parameter in the peritumoural region in differentiating SBM from HGG. Figures 3A, 3B, and 3C illustrate the ROC curve analysis results for all the parameters. Of all the parameters, rCBV had the highest individual distinctive power, with an AUC of 0.906.

Table 4 shows the sensitivity, specificity, PPV, NPV, and AUC values of the different combinations of DWI, DSCI, and MRS parameters used in differentiating SBM from HGG. Figure 4 illustrates the ROC curve analysis results for the combinations of the DWI, DSCI, and MRS parameters. In differentiating between these two tumours, any one of the model combinations (Fig. 4) was superior to using any individual DWI, DSCI, and MRS parameter (Fig. 3A, B). The best model in differentiating SBM from HGG was the combination of ADCmin, rCBV, and Cho/NAA parameters, and the sensitivity, specificity, PPD, NPD, and AUC values were 94.1%, 100%, 100%, 97.4%, and 0.970, respectively.

Discussion

Our study showed that the individual use of any of the peritumoural DWI, DSCI, and MRS parameters can help differentiate SBM from HGG. HGG was distinguished from SBM in the peritumoural region using the ROC analysis. Any model combination was found to be superior to any individual DWI, DSCI, and MRS parameter, and the best model was the combination of the peritumoural ADCmin, rCBV and Cho/NAA parameters, with an AUC of 0.970. Our results indicate that peritumoural DWI, DSCI, and MRS parameter combinations can better explain the following hypothesis: HGG is spread by infiltration into the peritumoural area, whereas peritumoural oedema is mainly composed of vasogenic oedema in metastases.
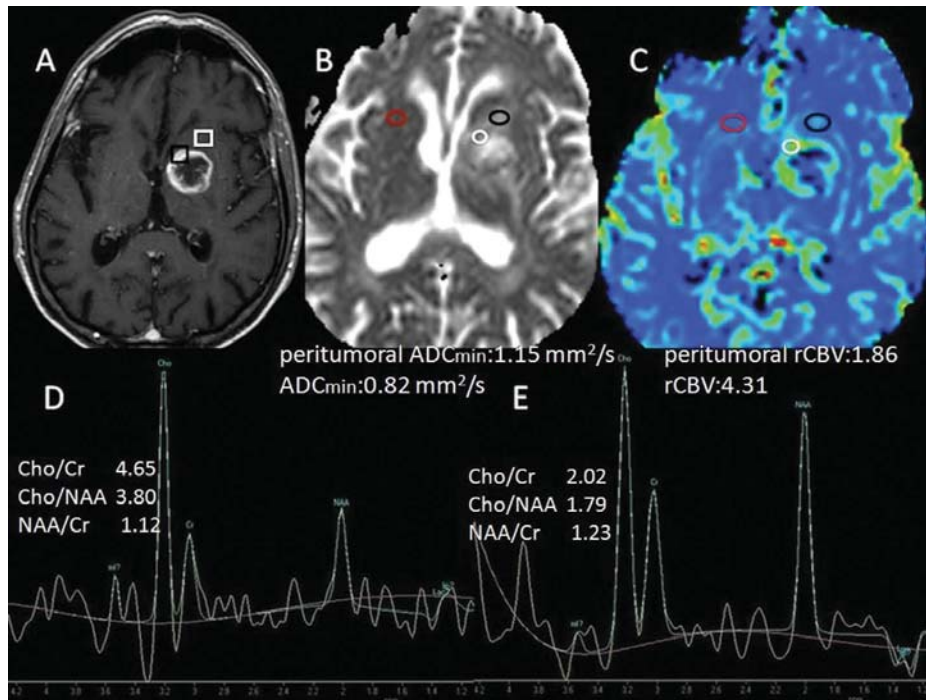
Figure 1. A 67 year-old male patient with pathologically confirmed glioblastoma. **A.** Contrast-enhanced T1-weighted image shows an irregular ring-like enhancement and a necrosis centralised mass in the left basal ganglion. Regions of interest localised in the enhancing tumour (white), peritumoural oedema (black), and contralateral white matter (red) are seen on the ADC map (B) and DSCI–CBV map (C). **B.** The ADC map shows low ADC values in the enhancing tumour and the peritumoural region, reflecting infiltrative oedema. The ADCmin, ADCmax, and ADCmean values for the enhancing tumour and the peritumoural region on the ADC map are 0.82, 1.07, and 0.96 × 10^{-3} mm^2/s and 1.15, 1.33, and 1.22 × 10^{-3} mm^2/s, respectively. **C.** The DSCI–CBV map shows increased rCBV (4.31 and 1.86, respectively) in the enhancing tumour and the peritumoural region, indicating infiltration. **D.** MRS (TE 144 ms) shows increased Cho/Cr (4.65 and 2.02, respectively) and Cho/NAA (3.80 and 1.79, respectively) and decreased NAA/Cr (1.12 and 1.23, respectively) in the enhancing tumour and the peritumoural region, indicating infiltration

The enhancing areas of both HGG and SBM are heterogeneous because of necrosis, haemorrhage, and vascular proliferation, and the normal parenchymal microstructure can be impaired. On the other hand, the peritumoural region is homogeneous because of the absence of necrosis and haemorrhage, and microstructural structure is relatively maintained [35, 40, 41]. In parallel with this, our results showed that in the enhancing tumour, all the parameters except NAA/Cr (P = 0.024) were not statistically different in differentiating HGG from SBM (P > 0.05).

DWI

The present study showed that the ADCmin, ADCmax, ADCmean, rADCmin, rADCmax, and rADCmean values of HGG in the peritumoural region are statistically low (for all ADC parameters, P < 0.001) compared to those of SBM, and these results are consistent with those of other studies [5-14]. Studies have reported that the peritumoural ADCmin values were superior to the ADCmax and ADCmean values in differentiating SBM from HGG [5, 13]. Similarly, our study found that the peritumoural ADCmin value (AUC:0.860) had greater diagnostic accuracy than the ADCmax (AUC:0.822),

ADCmean (AUC:0.848), rADCmin (AUC:0.822), rADCmax (AUC:0.801), and rADCmean (AUC:0.822) values in differentiating SBM from HGG. In differentiating between these two tumours, sensitivity was 82.4%, specificity was 89.7%, PPV was 77.8%, and NPV was 92.1% when the peritumoural ADCmin cutoff value was 1.32. Only a few studies have reported that the peritumoural ADC values were not statistically different between HGG and SBM [10, 38].

Tumour ADC (min, max, and mean) and rADC (min, max, and mean) did not show a statistical difference between HGG and SBM in our study (P > 0.05). These results were in accordance with the results of previous studies reporting that tumour ADC values are not useful in differentiating SBM from HGG [5–9, 11, 12]. However, some studies have shown that tumoural ADC values could help to differentiate SBM from HGG [10, 14, 28, 33, 34]. The inconsistencies among studies that included ADC values in the differentiation between these two tumours could be secondary to the differences in the underlying tumour histology and different degrees of tumour heterogeneity in the contrasted area caused by necrosis, calcification, and haemorrhage. The results of this study support the hypothesis that peritumoural ADC values
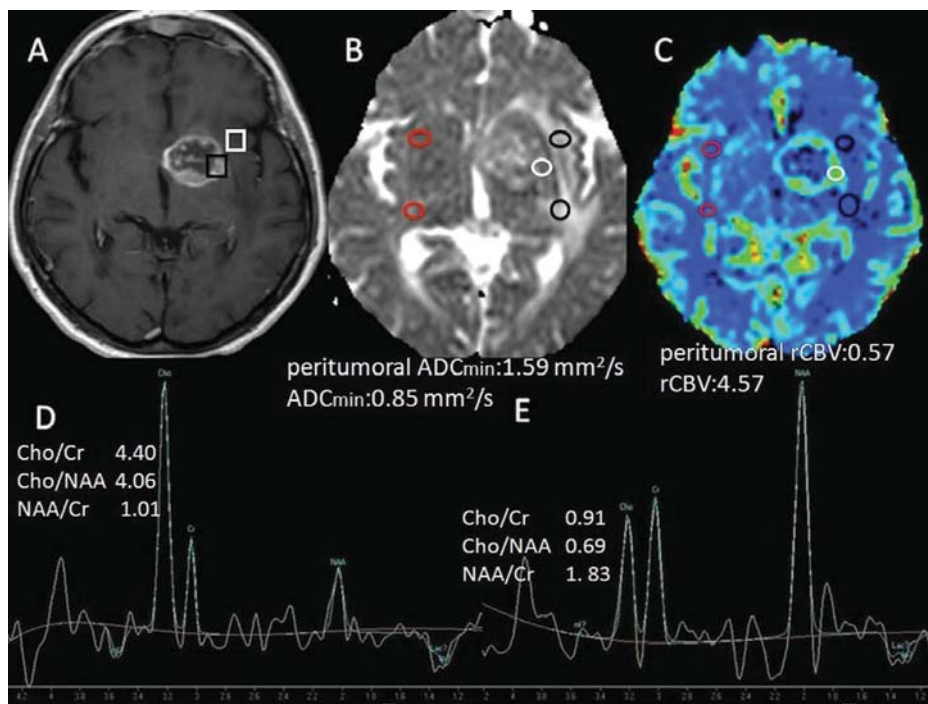
Figure 2. A 67 year-old male patient with pathologically confirmed pulmonary adenocarcinoma metastasis. **A.** Contrast-enhanced T1-weighted image shows an irregular ring-like enhancement and a necrosis centralised mass in the left basal ganglion. Regions of interest localised in the enhancing tumour (white), peritumoural oedema (black), and contralateral white matter (red) are seen on the ADC map (B) and the DSCI–CBV map (C). **B.** The ADC map shows low ADC values in the enhancing tumour but high ADC values in the peritumoural region, thus indicating vasogenic oedema. The ADCmin, ADCmax, and ADCmean values for the enhancing tumour and the peritumoural region on the ADC map are 0.85, 1.04, and 0.93 × 10^{-3} mm²/s and 1.59, 1.76, and 1.64 × 10^{-3} mm²/s, respectively. **C.** The DSCI–CBV map shows increased rCBV in the enhancing tumour but decreased rCBV in the peritumoural region, thus reflecting vasogenic oedema (4.57 and 0.57, respectively). **D.** MRS (TE 144 ms) shows increased Cho/Cr (4.40) and Cho/NAA (4.06) in the enhancing tumour and decreased Cho/Cr (0.91) and Cho/NAA (0.69) in the peritumoural region, thus reflecting vasogenic oedema, and decreased NAA/Cr (1.01 and 1.83, respectively) in both

Table 1. DWI, MRS, DSCI parameter values for the enhancing tumour in SBM and HGG

Parameter	Solitary Brain Metastasis		High-grade Glioma		p value	κ
	Mean ± SD	Median (min-max)	Mean ± SD	Median (min-max)		
ADCmin	0.83 ± 0.20	0.81 (0.56–1.31)	0.85 ± 0.15	0.82 (0.59–1.39)	> 0.05	0.856
ADCmax	1.08 ± 0.21	1.00 (0.82–1.62)	1.09 ± 0.16	1.05 (0.88–1.69)	> 0.05	0.911
ADCmean	0.95 ± 0.20	0.92 (0.70–1.42)	0.97 ± 0.15	0.94 (0.70–1.40)	> 0.05	0.814
rADCmin	1.16 ± 0.28	1.12 (0.78–1.81)	1.18 ± 0.21	1.13 (0.81–1.92)	> 0.05	0.713
rADCmax	1.37 ± 0.26	1.27 (1.04– 2.06)	1.38 ± 0.21	1.34 (1.11–2.15)	> 0.05	0.798
rADCmean	1.21 ± 0.26	1.17 (0.89–1.80)	1.24 ± 0.19	1.24 (0.89–1.78)	> 0.05	0.756
rCBV	3.68 ± 1.40	3.24 (1.88–7.41)	3.63 ± 1.40	3.29 (1.65–8.07)	> 0.05	0.895
Cho/Cr	4.42 ± 2.44	3.67 (1.57–11.26)	3.55 ± 1.71	3.12 (1.23–9.68)	> 0.05	0.969
Cho/NAA	3.15 ± 1.89	2.97 (0.77–8.11)	3.49 ± 1.77	3.03 (1.46–10.12)	> 0.05	0.971
NAA/Cr	1.48 ± 0.51	1.54 (0.44–2.51)	1.08 ± 0.49	1.01 (0.27–2.08)	= 0.024	0.922

*Except for the *p*-values, and κ coefficient (κ); minimum, maximum, and mean apparent diffusion coefficient (ADCmin, ADCmax, and ADCmean), cerebral blood volume (rCBV), Choline/creatine (Cho/Cr), Choline/N-acetyl aspartate (Cho/NAA), and N-acetyl aspartate/creatine (NAA/Cr)

Table 2. DWI, MRS, DSCI parameter values for the peritumoural region in SBM and HGG*

Parameter	Solitary Brain Metastasis		High-grade Glioma		p value	κ
	Mean ± SD	Median (min-max)	Mean ± SD	Median (min-max)		
ADCmin	1.47 ± 0.16	1.45 (1.17–1.78)	1.12 ± 0.18	1.11 (0.70–1.51)	< 0.001	0.926
ADCmax	1.61 ± 0.17	1.59 (1.27–1.90)	1.31 ± 0.22	1.30 (0.82–1.88)	< 0.001	0.872
ADCmean	1.52 ± 0.16	1.51 (1.19–1.81)	1.20 ± 0.21	1.19 (0.74–1.69)	< 0.001	0.894
rADCmin	1.85 ± 0.22	1.85 (1.44–2.26)	1.43 ± 0.25	1.41 (0.87–1.91)	< 0.001	0.764
rADCmax	2.05 ± 0.22	2.02 (1.62–2.42)	1.67 ± 0.28	1.65 (1.05–2.38)	< 0.001	0.685
rADCmean	1.93 ± 0.20	1.91 (1.51–2.30)	1.52 ± 0.28	1.51 (0.94–2.15)	< 0.001	0.712
rCBV	0.39 ± 0.18	0.39 (0.05–0.74)	1.14 ± 0.46	1.13 (0.47–2.53)	< 0.001	0.822
Cho/Cr	1.05 ± 0.21	1.05 (0.66–1.44)	1.79 ± 0.26	1.72 (0.88–2.68)	< 0.001	0.952
Cho/NAA	0.72 ± 0.21	0.69 (0.46–1.22)	1.72 ± 0.22	1.70 (1.46–2.54)	< 0.001	0.965
NAA/Cr	1.69 ± 0.51	1.67 (0.87–2.81)	1.26 ± 0.41	1.21 (0.63–2.47)	= 0.009	0.928

*Except for the *p*-values, and κ coefficient (κ); minimum, maximum, and mean apparent diffusion coefficient (ADCmin, ADCmax, and ADCmean), cerebral blood volume (rCBV), Choline/creatine (Cho/Cr), Choline/N-acetyl aspartate (Cho/NAA), and N-acetyl aspartate/creatine (NAA/Cr)

Table 3. Cutoff, sensitivity, specificity, PPV, NPV, and AUC values in differentiating between SBM and HGG in the peritumoural region with ROC

Parameter	Cutoff	Sensitivity	Specificity	PPV	NPV	AUC
ADCmin	1.32	82.4%	89.7%	77.8%	92.1%	0.860
ADCmax	1.48	82.4%	82.1%	66.7%	91.4%	0.822
ADCmean	1.44	82.4%	87.2%	73.7%	91.9%	0.848
rADCmin	1.67	82.4%	82.1%	66.7%	91.4%	0.822
rADCmax	1.86	82.4%	76.9%	60.8%	90.9%	0.801
rADCmean	1.79	82.4%	82.1%	66.7%	91.4%	0.822
rCBV	0.61	94.1%	87.2%	76.2%	97.1%	0.906
Cho/Cr	1.29	88.2%	82.1%	68.2%	94.1%	0.851
Cho/NAA	0.99	88.2%	92.3%	83.3%	94.7%	0.903
NAA/Cr	1.33	%82.4	74.4%	58.3%	90.6%	0.784

Area under the curve (AUC), minimum, maximum, and mean apparent diffusion coefficient (ADCmin, ADCmax, and ADCmean), cerebral blood volume (rCBV), Choline/creatine (Cho/Cr), Choline/N-acetyl aspartate (Cho/NAA), N-acetyl aspartate/creatine (NAA/Cr), positive predictive value (PPV), and negative predictive value (NPV)

Table 4. Sensitivity, specificity, PPV, NPV, and AUC values by using the combination of DWI, MRS, and DSCI parameters in differentiating between SBM and HGG in the peritumoural region with ROC

| Models	AUC	Sensitivity	Specificity	PPV	NPV
ADCmin+ rCBV	0.932	94.1%	92.1%	84.2%	97.2%
ADCmin+ Cho/NAA	0.941	88.2%	100%	100%	95.0%
rCBV+ Cho/NAA	0.941	88.2%	100%	100%	95.0%
ADCmin+ rCBV +Cho/NAA	0.970	94.1%	100%	100%	97.4%

Area under the curve (AUC), minimum apparent diffusion coefficient (ADCmin), cerebral blood volume (rCBV), Choline/N-acetyl aspartate (Cho/NAA), positive predictive value (PPV), and negative predictive value (NPV)

can determine neoplastic cell infiltration in the peritumoural oedema in HGG.

CBV

In this study, rCBV was higher in the peritumoural region in HGG than that in SBM (peritumoural rCBV was 1.14 and 0.39 for HGG and SBM, respectively, P < 0.001). This result is similar to those in previous studies [21–25, 32]. In addition, no significant difference was found in the tumour rCBV values between HGG and SBM (tumoural rCBV was 3.63 and 3.68 for HGG and SBM, respectively, P = 0.151). This result is consistent with those in previous studies reporting that tumour rCBV values are not useful in differentiating SBM from HGG [21–25, 32, 33]. When the peritumoural rCBV cutoff
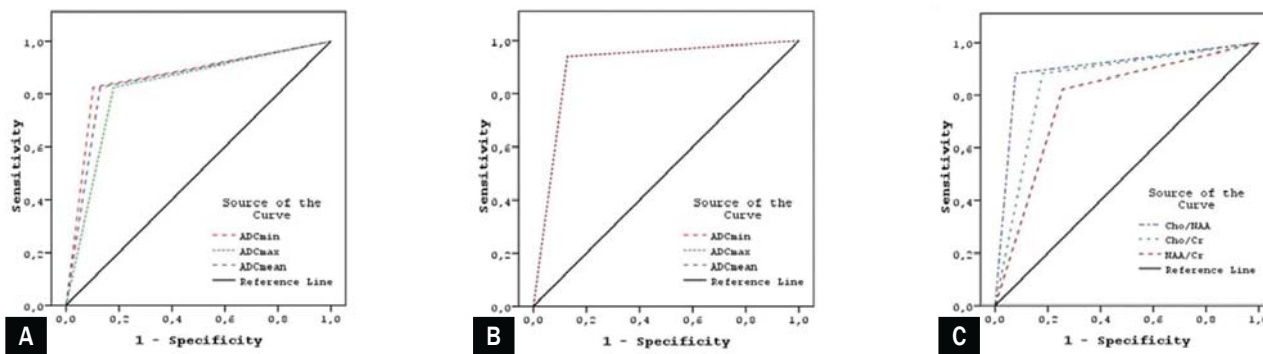
Figure 3. ROC analysis with AUC for each MR parameter when differentiating between SBM and HGG [AUC for DWI–ADCmin, ADCmax and ADCmean (**A**), DSCI–rCBV (**B**) and MRS–Cho/Cr, Cho/NAA, and NAA/Cr (**C**)]
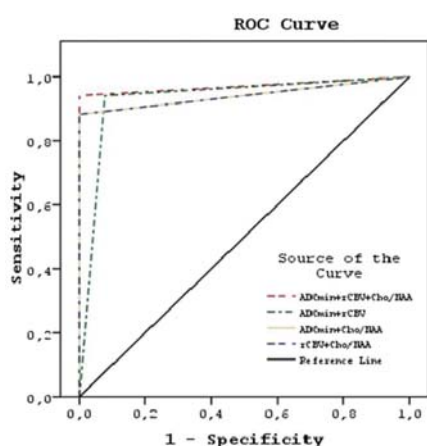
Figure 4. AUCs of different combinations of DWI, DSCI and MRS parameters in the peritumoural region with the ROC curve in differentiating SBM from HGG. The best model in differentiating between these two tumours was formed with the combination of ADCmin, rCBV, and Cho/NAA parameters

value was set to 0.61 in differentiating between these two tumours, sensitivity was 94.1%, specificity was 87.2%, PPV was 76.2%, and NPV was 97.1%. In differentiating between these two lesions, the highest individual power among all the parameters was rCBV, with an AUC of 0.906. Therefore, rCBV seems to be the best individual parameter to determine peritumoural invasion.

The rCBV rates, which are the biological indicator of angiogenesis obtained from peritumoural areas, showed pure vasogenic oedema in SBM despite exhibiting neoangiogenesis in HGG. Therefore, perfusion analysis of the peritumoural areas with DSCI can be considered reliable in differentiating between the two tumours.

MRS

The significant increase in peritumoural Cho/Cr [17, 18, 27, 28, 38] and Cho/NAA [18, 38, 42] rates of HGG compared to those of SBM (P < 0.001 for both) and the significant decrease in NAA/Cr [17, 37] rates (P = 0.009) in our study were similar to those in previous works. However, some studies have reported no significant differences in the peritumoural NAA/Cr rates between these two tumours [27, 28]. These results show the decrease in NAA based on neuron loss, which is a clear effect of peritumoural invasion in HGG, and the increase in total choline and Cho/NAA rates. These changes are not observed in the peritumoural regions of SBM [43, 44].

In the present study, a significant increase was reported in the NAA/Cr rates in the enhancing tumour in SBM compared to that in HGG (P = 0.024). The reason for this increase is probably the Cr deficiency in metastasis reported in previous studies [16] and the negative correlation between tumour infiltration degree and total tumour NAA [45]. This result is inconsistent with those of Law et al. [27] and Tsougos et al. [38], but is consistent with that of Server et al. [18]

No significant difference was found in the enhancing tumour Cho/Cr rates between HGG and SBM (P = 0.216), consistent with previous studies [28, 38, 42]. However, some studies have shown that the enhancing tumour Cho/Cr rates were lower in HGG than in SBM, and that this could be due to necrosis [18, 27]. In the present study, no significant difference was found in the enhancing tumour Cho/NAA rates between HGG and SBM (P = 0.358). This result agrees with those of previous studies [17, 38, 42]. The sensitivity and specificity values of peritumoural Cho/Cr, Cho/NAA, and NAA/Cr rates in differentiating HGG from SBM were 88.2% and 82.1%; 88.2% and 92.3%; and 82.4% and 74.4%, respectively. The highest individual power in all MRS parameters in differentiating between these two lesions was peritumoural Cho/NAA with an AUC of 0.903. This result is consistent was those of other studies [18, 38]. It also supports the finding in other studies that the Cho/NAA rate is associated with the proliferation of tumour cells [46, 47] and that choline exhibits cell density [48].

ROC analysis

We hypothesised that in differentiating HGG from SBM, advanced MRI techniques such as DWI, DSCI, and MRS, which can explain increased cellularity, density, and neoangiogenesis based on infiltration in the peritumoural region, could be closely associated with complicated and non-linear methods. Therefore, a combination of these MRI techniques could result in greater diagnostic accuracy. As each advanced MRI parameter can give limited information about the peritumoural region characteristic of the tumour (cellularity, density, and neo-angiogenesis), it can be insufficient in differentiating these two tumours.

A combination of multiple parameters can provide great diagnostic accuracy to differentiate between these two tumours. Recently, some researchers have examined the advantages of different combinations of advanced MRI techniques in differentiating SBM from HGG. Svalos et al. [32] combined diffusion (ADC and FA) and perfusion (rCBV) techniques with classification methods in differentiating glioblastomas and metastases from atypical meningiomas, and they reported that this combination provided additional diagnostic information in definitive diagnosis. Wang et al. [33] showed that DTI metrics and rCBV measurements could help in differentiating glioblastomas, brain metastases, and PCLs. In another study conducted with DTI, Wang et al. [34] reported that fractional anisotropy and mean diffusivity classification models could increase diagnostic performance in the contrasted lesion of tumour in differentiating glioblastomas from brain metastases. Bauer et al. [35] showed that the combination of MR diffusion and perfusion parameters was superior to the use of any individual parameter in differentiating SBM from glioblastoma multiforme. To the best of our knowledge, in the differentiation between HGG and SBM, quantitative MR parameter combinations with combined ROC curve analysis provided by DWI, DSCI, and MRS were not used in any of the previous studies. Our study showed that in differentiating HGG from SBM, any of the model combinations in the peritumoural region (Figure 4) had a higher diagnostic accuracy than the individual use of any of the DWI, DSCI, and MRS parameters (Figures 3A, B, C). With ROC analysis, our study showed that the best model that could differentiate HGG from SBM is the combination of peritumoural ADCmin, rCBV, and Cho/NAA parameters; the sensitivity, specificity, PPD, NPD, and AUC values were 94.1%, 100%, 100%, 97.4%, and 0.970, respectively. The combination of quantitative information provided by peritumoural DWI, DSCI, and MRS with ROC analysis methods can better explain the underlying pathophysiology (unlike vasogenic oedema, infiltrative oedema has high cellularity, density, and neo-angiogenesis) in the peritumoural region used in the differentiation of these two tumours. Also, additional diagnostic information provided by each parameter can be combined for improved diagnostic performance. Therefore, this hypothesis is confirmed by the combination of parameters with ROC curve analysis in the peritumoural area.

Limitations

Our study has some limitations. Firstly, as this work is a retrospective study, the ROIs placed in the enhancing tumour and in the peritumoural region did not match with the tissue places sampled for histological analysis. Further prospective studies that directly associate ROIs with histological observations are important, so that the DWI, DSCI, and MRS parameters can be more accurately interpreted. Secondly, this study has a small sample size. A large sample is required to confirm the results of our study. Thirdly, the signals of metabolites could have been influenced by partial volume effects in some cases because of the effects of tumour heterogeneity. Lastly, we did not use absolute metabolite assessment methods.

Conclusion

This study showed that the individual use of any of the peritumoral DWI, DSCI, and MRS parameters could be useful in differentiating between HGG and SBM. In differentiating HGG from SBM in the peritumoural region with ROC analysis, any of the model combinations was superior to any individual DWI, DSCI, and MRS parameter, and the best model found was the combination of peritumoural ADCmin, rCBV, and Cho/NAA, with 97% diagnostic accuracy. Therefore, the combination of peritumoural DWI, DSCI, and MRS parameters can provide more accurate diagnostic information in differentiating SBM from HGG.

References

1. Elmariah SB, Huse J, Mason B, et al. Multicentric glioblastoma multiforme in a patient with BRCA-1 invasive breast cancer. Breast J. 2006; 12(5): 470–474, doi: 10.1111/j.1075-122X.2006.00307.x, indexed in Pubmed: 16958968.

2. Single Brain Metastasis. Curr Treat Options Neurol. 2001; 3(1): 89–99, indexed in Pubmed: 11123862.

3. Campos S, Davey P, Hird A, et al. Brain metastasis from an unknown primary, or primary brain tumour? A diagnostic dilemma. Curr Oncol. 2009; 16(1): 62–66, indexed in Pubmed: 19229374.

4. Oh J, Cha S, Aiken AH, et al. Quantitative apparent diffusion coefficients and T2 relaxation times in characterizing contrast enhancing brain tumors and regions of peritumoral edema. J Magn Reson Imaging. 2005; 21(6): 701–708, doi: 10.1002/jmri.20335, indexed in Pubmed: 15906339.

5. Lee EJa, terBrugge K, Mikulis D, et al. Diagnostic value of peritumoral minimum apparent diffusion coefficient for differentiation of glioblastoma multiforme from solitary metastatic lesions. AJR Am J Roentgenol. 2011; 196(1): 71–76, doi: 10.2214/AJR.10.4752, indexed in Pubmed: 21178049.

6. Byrnes TJD, Barrick TR, Bell BA, et al. Diffusion tensor imaging discriminates between glioblastoma and cerebral metastases in vivo. NMR Biomed. 2011; 24(1): 54–60, doi: 10.1002/nbm.1555, indexed in Pubmed: 20665905.

7. Lu S, Ahn D, Johnson G, et al. Peritumoral diffusion tensor imaging of high-grade gliomas and metastatic brain tumors. AJNR Am J Neuroradiol. 2003; 24(5): 937–941, indexed in Pubmed: 12748097.

8. Pavlisa G, Rados M, Pavlisa G, et al. The differences of water diffusion between brain tissue infiltrated by tumor and peritumoral vasogenic edema. Clin Imaging. 2009; 33(2): 96–101, doi: 10.1016/j.clinimag.2008.06.035, indexed in Pubmed: 19237051.

9. Lemercier P, Paz Maya S, Patrie JT, et al. Gradient of apparent diffusion coefficient values in peritumoral edema helps in differentiation of glioblastoma from solitary metastatic lesions. AJR Am J Roentgenol. 2014; 203(1): 163–169, doi: 10.2214/AJR.13.11186, indexed in Pubmed: 24951211.

10. Server A, Kulle B, Maehlen J, et al. Quantitative apparent diffusion coefficients in the characterization of brain tumors and associated peritumoral edema. Acta Radiol. 2009; 50(6): 682–689, doi: 10.1080/02841850902933123, indexed in Pubmed: 19449234.

11. Huang J, Luo J, Peng J, et al. Cerebral schistosomiasis: diffusion-weighted imaging helps to differentiate from brain glioma and metastasis. Acta Radiol. 2017; 58(11): 1371–1377, doi: 10.1177/0284185116687173, indexed in Pubmed: 28090792.

12. Tan Y, Wang XC, Zhang H, et al. Differentiation of high-grade-astrocytomas from solitary-brain-metastases: Comparing diffusion kurtosis imaging and diffusion tensor imaging. Eur J Radiol. 2015; 84(12): 2618–2624, doi: 10.1016/j.ejrad.2015.10.007, indexed in Pubmed: 26482747.

13. Han C, Huang S, Guo J, et al. Use of a high b-value for diffusion weighted imaging of peritumoral regions to differentiate high-grade gliomas and solitary metastases. J Magn Reson Imaging. 2015; 42(1): 80–86, doi: 10.1002/jmri.24747, indexed in Pubmed: 25223489.

14. Caravan I, Ciortea CA, Contis A, et al. Diagnostic value of apparent diffusion coefficient in differentiating between high-grade gliomas and brain metastases. Acta Radiol. 2018; 59(5): 599–605, doi: 10.1177/0284185117727787, indexed in Pubmed: 28835111.

15. Suh CH, Kim HS, Jung SC, et al. Diffusion-Weighted Imaging and Diffusion Tensor Imaging for Differentiating High-Grade Glioma from Solitary Brain Metastasis: A Systematic Review and Meta-Analysis. AJNR Am J Neuroradiol. 2018; 39(7): 1208–1214, doi: 10.3174/ajnr. A5650, indexed in Pubmed: 29724766.

16. Ishimaru H, Morikawa M, Iwanaga S, et al. Differentiation between high-grade glioma and metastatic brain tumor using single-voxel proton MR spectroscopy. Eur Radiol. 2001; 11(9): 1784–1791, doi: 10.1007/s003300000814, indexed in Pubmed: 11511902.

17. Fan G, Sun B, Wu Z, et al. In vivo single-voxel proton MR spectroscopy in the differentiation of high-grade gliomas and solitary metastases. Clin Radiol. 2004; 59(1): 77–85, indexed in Pubmed: 14697379.

18. Server A, Josefsen R, Kulle B, et al. Proton magnetic resonance spectroscopy in the distinction of high-grade cerebral gliomas from single metastatic brain tumors. Acta Radiol. 2010; 51(3): 316–325, doi: 10.3109/02841850903482901, indexed in Pubmed: 20092374.

19. Crisi G, Orsingher L, Filice S. Lipid and macromolecules quantitation in differentiating glioblastoma from solitary metastasis: a short-echo time single-voxel magnetic resonance spectroscopy study at 3 T. J Comput Assist Tomogr. 2013; 37(2): 265–271, doi: 10.1097/RCT.0b013e318282d2ba, indexed in Pubmed: 23493217.

20. Wang Q, Zhang J, Xu W, et al. Role of magnetic resonance spectroscopy to differentiate high-grade gliomas from metastases. Tumour Biol. 2017; 39(6): 1010428317710030, doi: 10.1177/1010428317710030, indexed in Pubmed: 28631566.

21. Lehmann P, Saliou G, de Marco G, et al. Cerebral peritumoral oedema study: does a single dynamic MR sequence assessing perfusion and permeability can help to differentiate glioblastoma from metastasis? Eur J Radiol. 2012; 81(3): 522–527, doi: 10.1016/j. ejrad.2011.01.076, indexed in Pubmed: 21334839.

22. Server A, Orheim TE, Graff BA, et al. Diagnostic examination performance by using microvascular leakage, cerebral blood volume, and blood flow derived from 3-T dynamic susceptibility-weighted contrast-enhanced perfusion MR imaging in the differentiation of glioblastoma multiforme and brain metastasis. Neuroradiology. 2011; 53(5): 319–330, doi: 10.1007/s00234-010-0740-3, indexed in Pubmed: 20625709.

23. Blasel S, Jurcoane A, Franz K, et al. Elevated peritumoural rCBV values as a mean to differentiate metastases from high-grade gliomas. Acta Neurochir (Wien). 2010; 152(11): 1893–1899, doi: 10.1007/s00701-010-0774-7, indexed in Pubmed: 20799046.

24. Hakyemez B, Erdogan C, Gokalp G, et al. Solitary metastases and high-grade gliomas: radiological differentiation by morphometric analysis and perfusion-weighted MRI. Clin Radiol. 2010; 65(1): 15–20, doi: 10.1016/j.crad.2009.09.005, indexed in Pubmed: 20103416.

25. Halshtok Neiman O, Sadetzki S, Chetrit A, et al. Perfusion-weighted imaging of peritumoral edema can aid in the differential diagnosis of glioblastoma mulltiforme versus brain metastasis. Isr Med Assoc J. 2013; 15(2): 103–105, indexed in Pubmed: 23516772.

26. Suh CH, Kim HoS, Jung SC, et al. Perfusion MRI as a diagnostic biomarker for differentiating glioma from brain metastasis: a systematic review and meta-analysis. Eur Radiol. 2018; 28(9): 3819–3831, doi: 10.1007/s00330-018-5335-0, indexed in Pubmed: 29619517.

27. Law M, Cha S, Knopp EA, et al. High-grade gliomas and solitary metastases: differentiation by using perfusion and proton spectroscopic MR imaging. Radiology. 2002; 222(3): 715–721, doi: 10.1148/radiol.2223010558, indexed in Pubmed: 11867790.

28. Chiang IC, Kuo YT, Lu CY, et al. Distinction between high-grade gliomas and solitary metastases using peritumoral 3-T magnetic resonance spectroscopy, diffusion, and perfusion imagings. Neuroradiology. 2004; 46(8): 619–627, doi: 10.1007/s00234-004-1246-7, indexed in Pubmed: 15243726.

29. Fayed N, Modrego PJ. The contribution of magnetic resonance spectroscopy and echoplanar perfusion-weighted MRI in the initial assessment of brain tumours. J Neurooncol. 2005; 72(3): 261–265, doi: 10.1007/s11060-004-2180-6, indexed in Pubmed: 15937650.

30. Rollin N, Guyotat J, Streichenberger N, et al. Clinical relevance of diffusion and perfusion magnetic resonance imaging in assessing intra-axial brain tumors. Neuroradiology. 2006; 48(3): 150–159, doi: 10.1007/s00234-005-0030-7, indexed in Pubmed: 16470375.

31. Sparacia G, Gadde JA, Iaia A, et al. Usefulness of quantitative peritumoural perfusion and proton spectroscopic magnetic resonance imaging evaluation in differentiating brain gliomas from solitary brain metastases. Neuroradiol J. 2016; 29(3): 160–167, doi: 10.1177/1971400916638358, indexed in Pubmed: 26988081.

32. Svolos P, Tsolaki E, Kapsalaki E, et al. Investigating brain tumor differentiation with diffusion and perfusion metrics at 3T MRI using pattern recognition techniques. Magn Reson Imaging. 2013; 31(9): 1567–1577, doi: 10.1016/j.mri.2013.06.010, indexed in Pubmed: 23906533.

33. Wang S, Kim S, Chawla S, et al. Differentiation between glioblastomas, solitary brain metastases, and primary cerebral lymphomas using diffusion tensor and dynamic susceptibility contrast-enhanced MR imaging. AJNR Am J Neuroradiol. 2011; 32(3): 507–514, doi: 10.3174/ajnr.A2333, indexed in Pubmed: 21330399.

34. Wang S, Kim SJ, Poptani H, et al. Diagnostic utility of diffusion tensor imaging in differentiating glioblastomas from brain metastases. AJNR Am J Neuroradiol. 2014; 35(5): 928–934, doi: 10.3174/ajnr.A3871, indexed in Pubmed: 24503556.

35. Bauer AH, Erly W, Moser FG, et al. Differentiation of solitary brain metastasis from glioblastoma multiforme: a predictive multiparametric approach using combined MR diffusion and perfusion. Neuroradiology. 2015; 57(7): 697–703, doi: 10.1007/s00234-015-1524-6, indexed in Pubmed: 25845813.

36. Tsolaki E, Svolos P, Kousi E, et al. Automated differentiation of glioblastomas from intracranial metastases using 3T MR spectroscopic and perfusion data. Int J Comput Assist Radiol Surg. 2013; 8(5): 751–761, doi: 10.1007/s11548-012-0808-0, indexed in Pubmed: 23334798.

37. Mouthuy N, Cosnard G, Abarca-Quinones J, et al. Multiparametric magnetic resonance imaging to differentiate high-grade gliomas and brain metastases. J Neuroradiol. 2012; 39(5): 301–307, doi: 10.1016/j.neurad.2011.11.002, indexed in Pubmed: 22197404.

38. Tsougos I, Svolos P, Kousi E, et al. Differentiation of glioblastoma multiforme from metastatic brain tumor using proton magnetic resonance spectroscopy, diffusion and perfusion metrics at 3 T. Cancer Imaging. 2012; 12: 423–436, doi: 10.1102/1470-7330.2012.0038, indexed in Pubmed: 23108208.

39. Wu O, Østergaard L, Weisskoff RM, et al. Tracer arrival timing-insensitive technique for estimating flow in MR perfusion-weighted imaging using singular value decomposition with a block-circulant deconvolution matrix. Magn Reson Med. 2003; 50(1): 164–174, doi: 10.1002/mrm.10522, indexed in Pubmed: 12815691.

40. Rees JH, Smirniotopoulos JG, Jones RV, et al. Glioblastoma multiforme: radiologic-pathologic correlation. Radiographics. 1996; 16(6): 1413–38; quiz 1462, doi: 10.1148/radiographics.16.6.8946545, indexed in Pubmed: 8946545.

41. Long DM. Capillary ultrastructure in human metastatic brain tumors. J Neurosurg. 1979; 51(1): 53–58, doi: 10.3171/jns.1979.51.1.0053, indexed in Pubmed: 448419.

42. Weber MA, Zoubaa S, Schlieter M, et al. Diagnostic performance of spectroscopic and perfusion MRI for distinction of brain tumors. Neurology. 2006; 66(12): 1899–1906, doi: 10.1212/01.wnl.0000219767.49705.9c, indexed in Pubmed: 16801657.

43. Croteau D, Scarpace L, Hearshen D, et al. Correlation between magnetic resonance spectroscopy imaging and image-guided biopsies: semiquantitative and qualitative histopathological analyses of patients with untreated glioma. Neurosurgery. 2001; 49(4): 823–829, doi: 10.1097/00006123-200110000-00008, indexed in Pubmed: 11564242.

44. Wijnen JP, Idema AJS, Stawicki M, et al. Quantitative short echo time 1H MRSI of the peripheral edematous region of human brain tumors in the differentiation between glioblastoma, metastasis, and meningioma. J Magn Reson Imaging. 2012; 36(5): 1072–1082, doi: 10.1002/jmri.23737, indexed in Pubmed: 22745032.

45. Stadlbauer A, Gruber S, Nimsky C, et al. Preoperative grading of gliomas by using metabolite quantification with high-spatial-resolution proton MR spectroscopic imaging. Radiology. 2006; 238(3): 958–969, doi: 10.1148/radiol.2382041896, indexed in Pubmed: 16424238.

46. Guo J, Yao C, Chen H, et al. The relationship between Cho/NAA and glioma metabolism: implementation for margin delineation of cerebral gliomas. Acta Neurochir (Wien). 2012; 154(8): 1361–70; discussion 1370, doi: 10.1007/s00701-012-1418-x, indexed in Pubmed: 22729482.

47. Price SJ, Young AMH, Scotton WJ, et al. Multimodal MRI can identify perfusion and metabolic changes in the invasive margin of glioblastomas. J Magn Reson Imaging. 2016; 43(2): 487–494, doi: 10.1002/jmri.24996, indexed in Pubmed: 26140696.

48. Nafe R, Herminghaus S, Raab P, et al. Preoperative proton-MR spectroscopy of gliomas--correlation with quantitative nuclear morphology in surgical specimen. J Neurooncol. 2003; 63(3): 233–245, indexed in Pubmed: 12892229.